

A novel wave breaking framework to estimate air-sea gas transfer velocities

Sophia E. Brumer¹ and Christopher J Zappa²

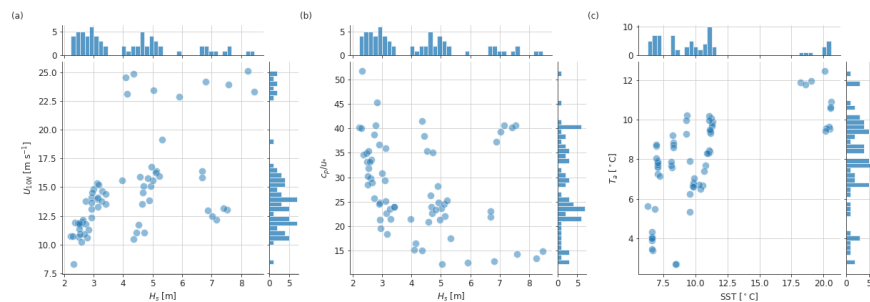
¹Univ. Brest, CNRS, IRD, Ifremer, Laboratoire d'Océanographie Physique et Spatiale (LOPS)

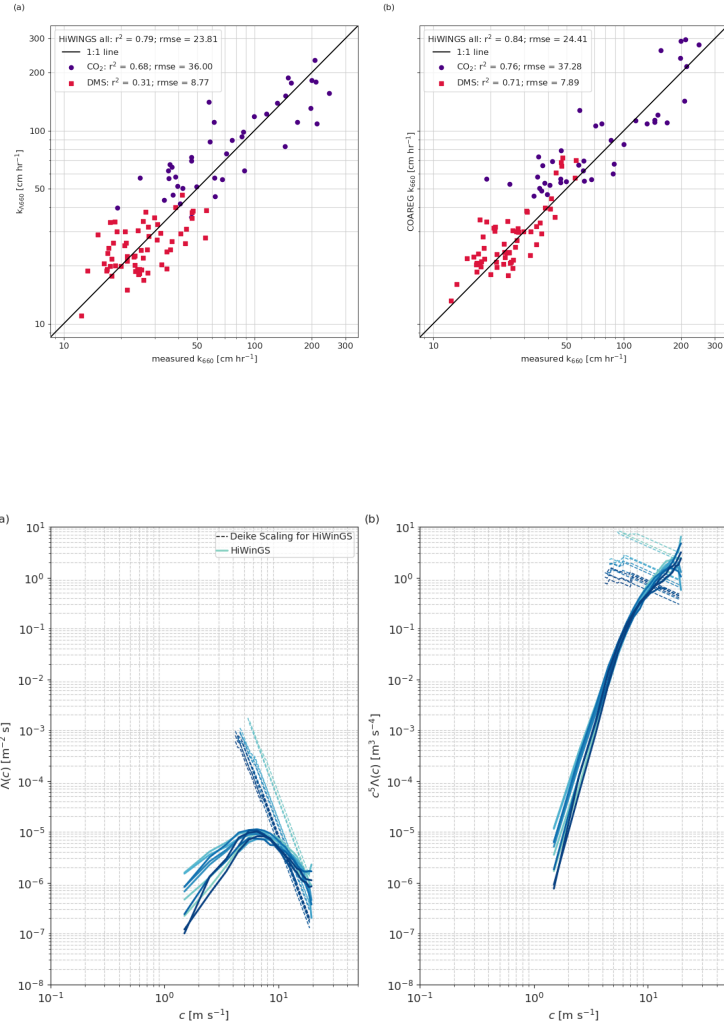
²Lamont-Doherty Earth Observatory of Columbia University

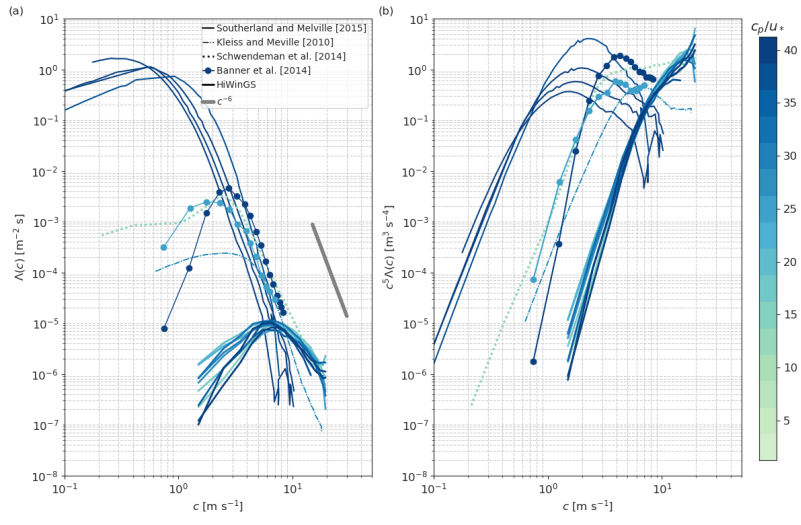
November 26, 2022

Abstract

Parameterizations of gas transfer velocities are needed for climate predictions. Single parameter models typically only include wind dependence and may readily be used in climate studies. Their application is however gas specific and limited to select environments. Mechanistic parameterizations incorporating multiple forcing factors allow modelling the transfer of gases with differing solubilities for a wide range of conditions. A novel framework is put forward to model gas transfer in the open ocean in the presence of breaking waves. It incorporates both the turbulence- and bubble-mediated transfers based on statistics determined from the breaking crest length distribution ($\lambda(c)$). Testing the mechanistic model with measurements from the HiWinGS field campaign shows promising results for both CO_2 and DMS. Uncertainties remain in the quantification of bubble clouds which are at the core of the formulation of the bubble-mediated transfer.







A novel wave breaking framework to estimate air-sea gas transfer velocities

Sophia E. Brumer^{1,a}, Christopher J. Zappa¹

¹Lamont-Doherty Earth Observatory of Columbia University, Palisades, NY, USA.

^aNow at Laboratoire d'Océanographie Physique et Spatiale, UMR 6523 CNRS-IFREMER-IRD-UBO,

IUEM, Plouzané, France

Key Points:

- a novel gas transfer velocity parameterization is proposed for wave breaking conditions
- modeling turbulence- and bubble-mediated gas transfer using breaking crest length distribution
- tested using breaking crest length distribution and gas flux measurements from HiWinGS

Corresponding author: Sophia E. Brumer, sophia.brumer@ifremer.fr

14 **Abstract**

15 Parameterizations of gas transfer velocities are needed for climate predictions. Single pa-
16 rameter models typically only include wind dependence and may readily be used in cli-
17 mate studies. Their application is however gas specific and limited to select environments.
18 Mechanistic parameterizations incorporating multiple forcing factors allow modelling the
19 transfer of gases with differing solubilities for a wide range of conditions. A novel frame-
20 work is put forward to model gas transfer in the open ocean in the presence of break-
21 ing waves. It incorporates both the turbulence- and bubble-mediated transfers based on
22 statistics determined from the breaking crest length distribution ($\Lambda(c)$). Testing the mech-
23 anistic model with measurements from the HiWinGS field campaign shows promising
24 results for both CO₂ and DMS. Uncertainties remain in the quantification of bubble clouds
25 which are at the core of the formulation of the bubble-mediated transfer.

26 **Plain Language Summary**

27 Predicting climate change relies on models of the transfer of gases across the atmosphere-
28 ocean interface. Traditionally for every gas a different function of wind speed is used to
29 compute its transfer velocity and air-sea flux. These functions are valid only in specific
30 environmental conditions. To improve predictions, models that account for the differ-
31 ent transfer mechanisms have to be developed. Ideally they are applicable to any gases
32 regardless of solubility. Such a model is put forward herein. It allows to estimate the trans-
33 fer velocities based on remote sensing of breaking waves and the wave field accounting
34 for both the transfer due to turbulence and bubbles. The model is tested with measure-
35 ments from the HiWinGS field campaign and shows promising results for both CO₂ and
36 DMS. Remaining uncertainties and limitations are discussed highlighting the need for
37 open ocean measurements of breaking waves and their associated bubble plume.

38 **1 Introduction**

39 Modelling air-sea gas fluxes is essential for climate predictions and relies on esti-
40 mates of the gas transfer velocity (k) which is typically parameterized as a function of
41 the 10-m wind speed (e.g. Wanninkhof, 1992; Ho et al., 2011). Large scatter is observed
42 in estimated gas transfer velocities (k) of sparingly soluble gases at high wind speeds where
43 wave breaking dominates upper ocean dynamics (Blomquist et al., 2017; Brumer et al.,
44 2017a). The removal of this scatter by a wind-wave based parameterization (Brumer et al.,

2017a) suggests that k would be better modeled with the inclusion of surface wave breaking rather than wind speed alone.

Wave breaking has the potential to considerably impact air-sea exchanges and upper-ocean dynamics (Deike, 2022). It leads to enhanced turbulent kinetic energy (TKE) in the near surface layer resulting in surface TKE dissipation rates (ε) shown to be roughly 5 to 1000 times greater than predicted by wall layer scaling (Agrawal et al., 1992; Gemmrich, 2010; Sutherland and Melville, 2015; Terray et al., 1996). Additionally, air-entraining breaking waves generate bubble clouds that allow for an additional pathway for gas transfer which is particularly important to consider for sparingly soluble gases such as CO_2 (Woolf, 1993).

Efforts have been made to account for the impact of bubbles in physical process based models (Deike and Melville, 2018; Fairall et al., 2011; Liang et al., 2013; Goddijn-Murphy et al., 2016; Asher et al., 1996). Only one of these models explicitly considers the contribution of wave breaking turbulence (Asher et al., 1996; Asher and Wanninkhof, 1998). However, it is reduced to a function of the whitecap cover and 10-m wind speed. None of these models include direct dependence of the transfer to the TKE dissipation due to wave breaking, it is implicitly comprised through dependence on the friction velocity amongst other forcing. While all these variables are inter-linked, it is not always in a straight forward way. The limitations of these models were revealed using the whitecap coverage and the gas transfer velocities of CO_2 and DMS observed during HiWinGS (Blomquist et al., 2017).

Several studies have shown how enhanced turbulence promotes gas transfer (Zappa et al., 2007; Tokoro et al., 2008; Vachon et al., 2010; Esters et al., 2017) but not in relation to breaking waves. Based on measurements of turbulence in the wave-affected and wave breaking layers, Shuiqing and Dongliang (2016) derived a parameterization for the gas transfer velocity in the presence of breaking waves. Their proposed functional form is similar to that of Asher and Wanninkhof (1998) without the bubble-mediated component. It does not directly depend on the turbulent kinetic energy dissipation rate, but rather the air friction velocity, the whitecap cover, and wave age.

Herein, a novel framework to model air-sea gas transfer velocities in the presence of breaking waves is put forth. The proposed framework incorporates both the turbulence- and bubble-mediated transfer. It is based on two statistics derived from the breaking crest

77 length distribution (Phillips, 1985): the turbulent kinetic energy dissipation rate and the
 78 bubble volume flux. Multiple field campaigns in the last decade have demonstrated the
 79 existence of a robust link between the breaking crest length distribution to the turbu-
 80 lent kinetic energy dissipation rate following the spectral framework proposed by Phillips
 81 (1985) to quantify wave breaking properties. Recently, through a combination of DNS
 82 and laboratory observations Deike et al. (2017) have extended the application of the Phillips
 83 (1985) framework allowing estimations of bubble cloud properties from the breaking crest
 84 length distribution. These advances are at the core of the present framework.

85 Section 2 provides an outline of the general form of the proposed model followed
 86 by a review of Phillips (1985)'s theoretical framework and the work of Deike et al. (2017)
 87 which are used for the derivation of quantities key to air-sea gas transfer. The model is
 88 tuned using data from the High Wind Gas Exchange Study (HiWinGS) which is shown
 89 in section 3. The model is compared to other existing physically-based models in sec-
 90 tions 4 where uncertainties and guidelines for future measurements are also discussed.

91 **2 Proposed Gas Transfer Model**

92 The proposed functional form of the k model accounting for the contribution of the
 93 turbulence-driven (k_ε) and the bubble-mediated (k_b) transfers is:

$$k = k_\varepsilon + k_b \quad (1)$$

94 Various mechanistic approaches were suggested by which turbulence promotes the trans-
 95 fer of gases. These invoke concepts of surface renewal (Higbie, 1935; Danckwerts, 1951;
 96 Lamont and Scott, 1970; Komori et al., 1993), surface penetration (Harriott, 1962; At-
 97 tmane et al., 2004) and surface divergence (McCready et al., 1986; Banerjee and Mac-
 98 Intyre, 2004; Banerjee et al., 2004; McKenna and McGillis, 2004; Turney et al., 2005)
 99 and their application is limited to a constrained set of environmental conditions. Bound-
 100 ary layer scaling arguments also allow to derive k_ε . The flux of gas (F_g) follows Fick's
 101 law of diffusion:

$$F_g = D \frac{\partial C}{\partial z} = \frac{D}{\delta_z} (C_w - \alpha C_a) = k_\varepsilon (C_w - \alpha C_a) \quad (2)$$

102 Where D is the diffusivity, δ_z a characteristic surface boundary length scale, α the Ost-
 103 wald solubility coefficient and C_a , C_w the air and water concentrations, respectively. This
 104 allows rewriting k_ε as:

$$k_\varepsilon = \frac{D}{\delta_z} \quad (3)$$

105 Using the Batchelor length scale $\delta_Z \propto \left(\frac{\nu_w D^2}{\varepsilon}\right)^{\frac{1}{4}}$, which is the characteristic turbulent
 106 microscale for a passive scalar (Batchelor, 1959), the following relationship between k_ε
 107 and ε was derived (Banerjee et al., 1968; Kitaigorodskii, 1984):

$$k_\varepsilon \propto (\varepsilon \nu_w)^{\frac{1}{4}} Sc^{-0.5} \quad (4)$$

108 where ν_w is the water viscosity, and $Sc(= \nu_w/D)$ is the water-side Schmidt number de-
 109 fined as the ratio of the water viscosity and the mass diffusivity D .

110 The bubble-mediated transfer is commonly expressed as function of the bubble vol-
 111 ume flux (F_a) or the void fraction (v) (Woolf, 1997; Woolf et al., 2007). Neglecting po-
 112 tential collective effects of bubbles Woolf proposed the so-called ‘‘independent bubble
 113 model’’:

$$k_{b_{ind}} \propto F_a \alpha^{-1} \left(1 + (\chi)^{1/1.2}\right)^{-1.2} \quad (5)$$

114 with

$$\chi \propto Sc^{-0.5} F_a \alpha^{-1} \quad (6)$$

115 It satisfies the two commonly accepted distinct asymptotic behaviours of k_b : 1) for highly
 116 soluble gases ($\alpha \gg 1$), where full equilibration is achieved, the bubble-mediated flux
 117 is limited by the bubble volume flux and solubility and 2) for very weakly soluble gases
 118 ($\alpha \ll 1$), where no equilibration is achieved, the flux does not depend on solubility
 119 but on diffusion (see also Keeling (1993); Goddijn-Murphy et al. (2016); ?).

120 Based on laboratory work by Cipriano and Blanchard (1981), Woolf (1997) first
 121 suggests that:

$$F_a = 6.25 \times W \text{ [m(m}^2 \text{ s)}^{-1}] = 2250 \times W \text{ [cm hr}^{-1}] \quad (7)$$

122 and

$$\chi = \frac{Sc^{-0.5}}{14\alpha} \quad (8)$$

123 Where W is the total whitecap cover expressed as a fraction. Later in the paper, Woolf
 124 uses $F_a = 2450W$ which is the value adopted by subsequent studies. Note that Eq. (8)
 125 removes the additional higher order F_a dependence of Eq. (5).

126 **2.1 Phillips’ [1985] Spectral Framework**

127 Laboratory experiments by Duncan (1981, 1983), in which a breaking wave was cre-
 128 ated by a hydrofoil towed at constant speed and depth, revealed a relationship between

129 energy dissipated by a steady breaking wave and its speed:

$$\varepsilon_l \propto \frac{\rho_w c_h^5}{g}, \quad (9)$$

130 where ε_l is the energy dissipation per crest length, ρ_w is the water density, g is the grav-
 131 itational acceleration, and c_h the speed of a towed hydrofoil which corresponds to the
 132 speed of the breaking crest, $c_h \sim c_{br}$.

133 Phillips (1985) introduced the spectral density of the breaking crest length per unit
 134 area $\Lambda(c)$, where c is the breaking wave phase speed. Based on Duncan's experiments,
 135 he proposed:

$$\varepsilon = \int S_{ds}(c)dc = \int b(c)\rho_w g^{-1}c^5\Lambda(c)dc \quad (10)$$

136 where S_{ds} is the spectral dissipation term from the radiative transfer equation that de-
 137 scribes the evolution of the wave field and $b(c)$ is the spectral breaking strength.

138 Recognizing the value of the breaking crest length distribution to infer breaking
 139 wave characteristics and subsequently air-sea interaction processes, multiple studies have
 140 been undertaken to obtain direct measurements of both $\Lambda(c)$ and ε . The first measure-
 141 ments of $\Lambda(c)$ were made by Phillips et al. (2001) using a marine radar. Later studies
 142 have used digital video camera to track breaking waves from stable platforms (Gem-
 143 rich et al., 2008, 2013; Schwendeman et al., 2014; Sutherland and Melville, 2013, 2015;
 144 Thomson et al., 2009; Zappa et al., 2012) and planes (Kleiss and Melville, 2010). Tech-
 145 niques to derive the breaking crest length distribution from the imagery vary greatly. These
 146 are reviewed and discussed in Banner et al. (2014). Here, the initial velocity method is
 147 adopted, in which the phase velocity c is equated to a fixed reference velocity that cor-
 148 responds to initial breaker-front velocity of each breaking event (c_{br}) as was originally
 149 chosen by Phillips (1985). The phase speed of the breaking wave has been shown to be
 150 closely related to the speed of the breaking crest c_{br} with $c_{br}/c \sim 0.8 - 0.9$. Following
 151 Gemmrich et al. (2008, 2013), the breaking crest length distribution $\Lambda(c_{br})$ for a given
 152 speed range ($c_{br}, c_{br} + \Delta c_{br}$) is then obtained from:

$$\Lambda(c_{br}) = \sum L_{br}t_{br}/(TA\Delta c_{br}) \quad (11)$$

153 where L_{br} is the characteristic breaking segment length, t_{br} duration of an individual break-
 154 ing crest event (based on the time a breaker is tracked in the imagery), A is the area of
 155 the field of view, and T the total duration of observation.

156 2.2 Estimating the turbulent kinetic energy dissipation rate

157 To estimate the turbulent kinetic energy dissipation rate from the breaking crest
 158 length distribution (Eq. 10), one unknown remains: the spectral breaking strength $b(c)$.
 159 Wave systems produced in laboratory experiments are narrow-banded and $b(c)$ is assumed
 160 to be independent of scale. It was found to vary with wave steepness (Banner and Peir-
 161 son, 2007; Drazen et al., 2008; Melville, 1994). Ocean waves are however rarely narrow-
 162 banded and modeling studies suggest that $b(c)$ may scale with wave age (Romero et al.,
 163 2012).

164 No direct field measurements of $b(c)$ exist to date as $\varepsilon(c)$ has not been tractable
 165 in the open ocean. A scale-independent effective breaking strength coefficient (b_{eff}) was
 166 thus defined:

$$b_{eff} = \frac{\varepsilon}{\rho_w g^{-1} \int c^5 \Lambda(c) dc} \quad (12)$$

167 Leading to:

$$\varepsilon(c) = b_{eff} c^5 \Lambda(c) / g \quad (13)$$

168 Reviewing all existing breaking crest length distribution and coinciding upper ocean dis-
 169 sipation rate measurements, Zappa et al. (2016) determined the following wave-age de-
 170 pendent parameterisation of b_{eff} :

$$b_{eff} = 3.48 \times 10^{-3} - 4.69 \times 10^{-5} \frac{c_p}{u_*} \quad (14)$$

171 Here c_p is the phase speed of the dominant wave and u_* the air friction velocity.

172 2.3 Estimating the Bubble Volume flux

173 Estimation of the bubble volume flux and void fractions are based on relations de-
 174 termined from novel direct numerical simulations (DNS) of three-dimensional breaking
 175 waves that resolve bubble scales (Deike et al., 2016). One of the key finding from this
 176 DNS study is that total volume of air entrained by a breaking wave (V_a) is directly pro-
 177 portional to the breaking crest length (L_{br}) and the breaking speed to the power 5:

$$V_a = B b_{eff} \frac{L_{br} c_{br}^5}{U_b g^2} \quad (15)$$

178 Where B is a dimensionless constant, and U_b is a dissipation-weighted vertical mean ve-
 179 locity which corresponds to the average rise velocity of the bubble plume. This relation
 180 stems from the core assumption that the global (integrated breaking event's spatio-temporal

181 extent) work done against buoyancy forces in entraining the bubbles is proportional to
 182 the mechanical energy dissipated where $B = 0.1$ is the proportionality factor. U_b scales
 183 as the rise velocity in clean water (Woolf and Thorpe, 1991) of a bubble of radius equal
 184 to the mean of the bubble distribution. Not knowing the bubble distribution, a constant
 185 U_b equal to 10 cm s^{-1} is assumed here based on Asher et al. (1997).

186 From Eq. 15, a volume flux per unit area (F_a) can be estimated by summing the
 187 total volume of air entrained by each breaker observed during a single video recording
 188 and dividing by the area of the field of view (A) and the total time of observations (T).

$$F_a = \frac{\sum V_a}{AT} = b_{eff} B \frac{\sum L_{br} c_{br}^5}{AT U_b g^2} \quad (16)$$

189 Alternatively, F_a may be expressed as a combination of the fifth moment of the break-
 190 ing crest length distribution and the breaking duration (τ_{br}):

$$F_a = \frac{b_{eff} B}{U_b g^2} \int \frac{1}{\tau_{br}(c)} \Lambda(c) c^5 dc \quad (17)$$

191 This form assumes that the duration of the breaker is a function of the breaker speed.
 192 As proposed by Kleiss (2009), based on laboratory and field data (Thorpe and Hall, 1983;
 193 Rapp and Melville, 1990), τ_{br} can be related to the period of the breaking wave which
 194 may be expressed in terms of the phase speed c via the deep water dispersion relation:

$$\tau_{br} \propto \frac{2\pi}{g} c \quad (18)$$

195 Kleiss (2009) suggests $\tau_{br} = 0.25 c_{br}$, thus:

$$F_a = 4 \frac{b_{eff} B}{U_b g^2} \int \Lambda(c) c^4 dc \quad (19)$$

196 2.4 Calibrating the Model Framework

197 As it is the case for all existing gas transfer model, several proportionality constants
 198 remain to be determined. This can be done by solving:

$$k_\Lambda = \mathcal{A} K_\epsilon + \mathcal{B} K_b \quad (20)$$

199 Where K_ϵ is equal to the right hand side of the relations in Eq. (4) and

$$K_b = F_a \alpha^{-1} \left(1 + (\mathcal{C} S c^{-0.5} F_a \alpha^{-1})^{1/1.2} \right)^{-1.2} \quad (21)$$

200 The coefficients \mathcal{A} , \mathcal{B} , and \mathcal{C} should be obtained through least squared error regression
 201 using measurements derived transfer velocities of gases of varying solubilities over a wide
 202 range of wind and wave conditions.

203 3 HiWinGS application

204 The proposed framework was tuned using the gas transfer velocities of CO₂ and
 205 DMS derived from the eddy co-variance measurements taken during the 2013 HiWinGS
 206 field campaign. Details about HiWinGS can be found in (Blomquist et al., 2017; Brumer
 207 et al., 2017a,b; Yang et al., 2014). Breaking waves were monitored through high frequency
 208 video recording of 20 minutes in the visible band throughout the daytime. Momentum,
 209 heat, and gas fluxes were computed hourly. Figure 1 illustrates the variable space sam-
 210 pled during the experiment where concurrent good quality data is available. Hourly av-
 211 eraged 10-m neutral wind speed (U_{10N}) range from 8.3 to 25.1 m s⁻¹, the significant wave
 212 height (H_s) from 2.2 to 8.5 m for wave ages (c_p/u_*) of 12.2 to 51.7. The sea surface (SST)
 213 and air (T_a) temperatures ranged 6.3-20.6 and 2.7-12.5°C, respectively with differences,
 214 $\Delta T = T_a - \text{SST}$ spanning -10.9 to 1.8°C.

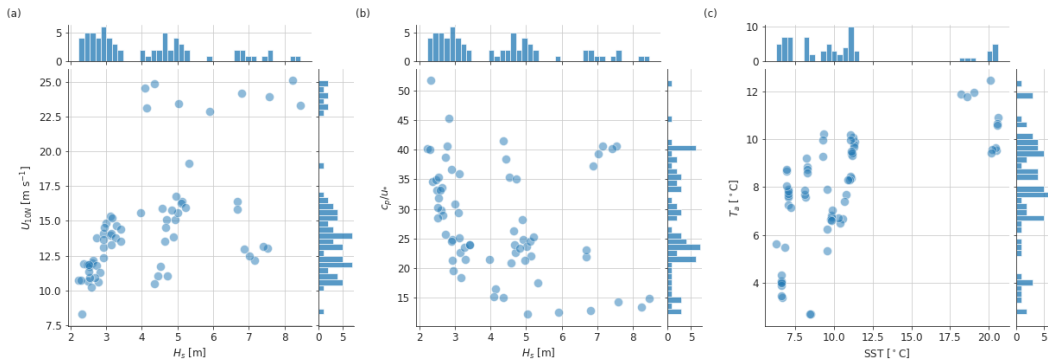


Figure 1. Scatter plots and histograms of (a) the neutral 10-m wind speed (U_{10N}) vs. the significant wave height (H_s), (b) the wave age (c_p/u_*) vs. the significant wave height, and (c) the surface air temperature (T_a) vs. the sea surface temperature (SST)

215 3.1 Tracking breaking crests

216 The breaking crest length distributions were determined from over 200 videos taken
 217 the starboard side of the flying bridge of the R/V Knorr. For details on the setup see
 218 Brumer et al. (2017b). All background gradients present in the images were removed prior
 219 to any further analysis. The images were then corrected for lens distortion and re-projected
 220 using the roll, pitch, and yaw angles measured by IMUs. Finally, they were interpolated

221 onto a regular grid with pixel resolution of 0.1 m. The area of the field of view A was
 222 $\sim 1100 \text{ m}^2$ and the total duration of observation T was around 19 minutes.

223 The breaking crest lengths were tracked following the method developed by Gemm-
 224 rich et al. (2008). In order to bring out the advancing side of the whitecap two consec-
 225 utive rectified and projected images are differenced. As whitecaps are brighter than the
 226 background, the advancing front is distinguishable by high positive values, while the rear
 227 side is negative in the differenced image. The differenced images are thresholded based
 228 on image intensity (I) using $I/\max(I) > 0.6$ and transformed into binary images where
 229 the breaking crests have pixels equal to 1 and the rest is set to 0.

230 Using Matlab's image processing toolbox, a series of morphological operations are
 231 then applied to the binary frames to insure that crest do not contain holes and to link
 232 crests that are close together into a single one (details in Supplementary Information (SI)).
 233 Finally, each crest is identified and approximated as an ellipse. This allows to determine
 234 the coordinates of the center of mass of each crest, as well as the length major and mi-
 235 nor axis, their area, and orientation.

236 At this stage crests that have an area smaller than 1.5 m^2 are removed. The re-
 237 maining crests are then tracked from one differenced frame to the next. Matching the
 238 crests in consecutive differenced frames is based on:

- 239 1. propagation direction of the centers of mass of $\pm 90^\circ$ relative to the ship's orien-
 240 tation which was pointed into the wind.
- 241 2. a propagation speed less than 1.2 times the phase speed of the waves at spectral
 242 peak.
- 243 3. change in area and major axis length less than 25%
- 244 4. orientations of the major axes within 15°

245 The theoretical minimum detectable crest advancement speed is dictated by the
 246 pixel resolution and the frame rate. A breaking crest can be seen to move from one frame
 247 to the next only if it traveled at least the equivalent distance of 1 pixel (0.1 m) in be-
 248 tween acquisition (1/20 s). Thus, at the native frame rate only waves traveling at a min-
 249 imum speed of 2 m s^{-1} are detectable. To reduce the resolvable propagation speed to 1
 250 m s^{-1} , breaking waves were tracked in every other image. Note, however, that the coor-

251 dinates of the center of masses are determined within fractions of pixels thus propaga-
 252 tion speeds smaller than 1 m s^{-1} can result from the analysis.

253 **3.2 Breaking crest length distributions**

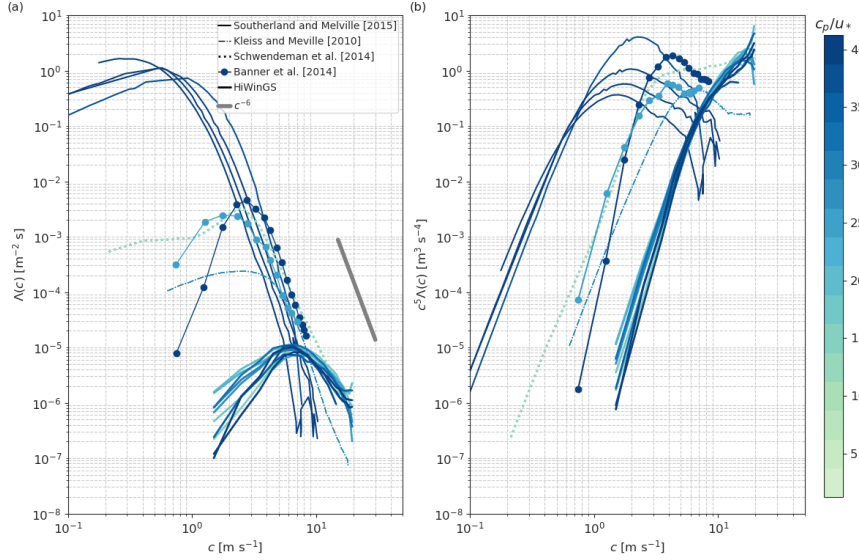


Figure 2. (a) Breaking crest length distributions and (b) their fifth moment as a function of the breaking crest speed color-coded by wave age ($\frac{c_p}{u_*}$).

254 Figure 2a shows the breaking crest length distributions as a function of the break-
 255 ing speed computed from the HiWinGS data set color-coded by wave age ($\frac{c_p}{u_*}$). Figure
 256 2b shows their fifth moment. Also shown are some of the previous breaking crest length
 257 determined from visible imagery. Much younger seas and higher winds were sampled dur-
 258 ing HiWinGS than during most of the previous field experiments outlined above. It is
 259 also important to note that different analysis techniques were used by the different groups.
 260 Only the two RaDyO datasets presented in Gemmrich et al. (2013) were analyzed with
 261 the technique used here. Mean breaking crest length distributions from Gemmrich’s anal-
 262 ysis are reported in Banner et al. (2014) and shown in 2. The discrepancies arising from
 263 the various analysis techniques and choices in independent variables (in particular c_{br})
 264 used to compute the breaking crest length distributions were highlighted by Banner et al.
 265 (2014) and will not be discussed further here. Nevertheless, these systematic differences

266 have to be taken into consideration when comparing the breaking crest length distribu-
 267 tions plotted here. The breaking crest length distribution computed from the HiWinGS
 268 data follow less closely the theoretical c^{-6} high c_{br} tail than previously published ones.
 269 This means that scalings for Λ such as those proposed by Sutherland and Melville (2013)
 270 or Deike and Melville (2018) poorly reproduce them (c.f. SI). There is no clear expla-
 271 nation for this discrepancy at this time.

272 3.3 Determining the Framework's Coefficients

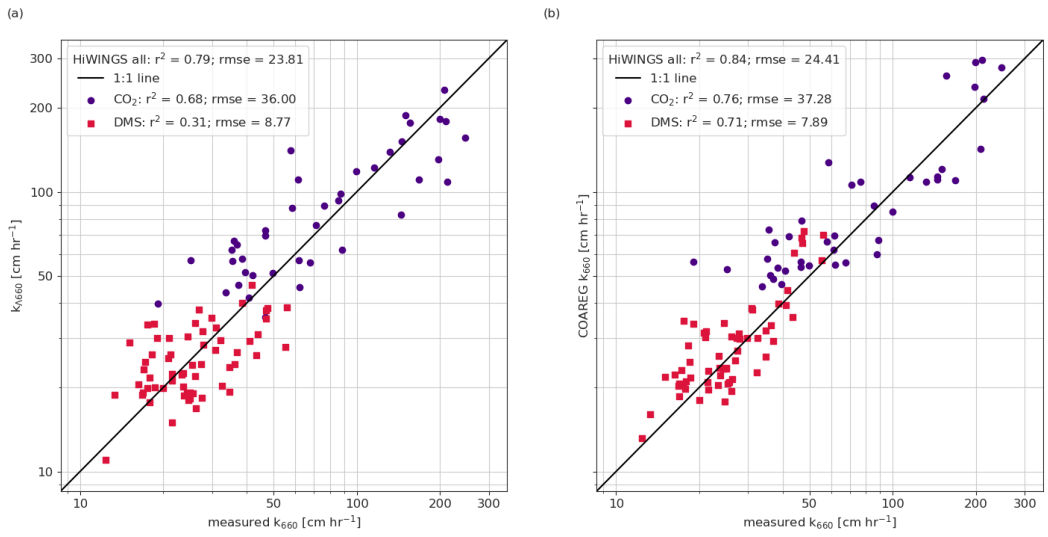


Figure 3. Scatter plots of (a) the k_{Λ} model proposed in Eq. 20: $k_{\Lambda 600} = 0.21K_{\epsilon} + 3.26F_a\alpha^{-1} \left(1 + (0.088Sc^{-0.5}F_a\alpha^{-1})^{1/1.2}\right)^{-1.2}$ and (b) the COAREG model (see SI for equations) versus the gas transfer velocities of CO₂ (purple) and DMS (ruby) estimated from HiWinGS eddy-covariance flux measurements referenced to a Schmidt number of 660.

273 A non-linear least squares fit of the HiWinGS data within the proposed breaking
 274 framework for the gas transfer velocity k_{Λ} (Eq. 20) provides $\mathcal{A} = 0.211 \pm 0.034$, $\mathcal{B} =$
 275 3.26 ± 0.574 , and $\mathcal{C} = 0.088 \pm 0.072$. Variability linked to the b_{eff} parameterization (Eq.
 276 13) was propagated. Results are shown in Figure 3a. k_{Λ} from Equation 20 is able ex-
 277 plain 79% of the overall variability in the measurement derived gas transfer velocities.
 278 The correlations to the transfer velocities of CO₂ ($r^2 = 0.68$) and DMS ($r^2 = 0.31$) in-
 279 individually are lower than for the overall fit, particularly for DMS. Output of NOAA's

280 COAREG algorithm (Blomquist et al. (2017); Fairall et al. (2011); equations in SI) for
 281 matching measurements are shown in Figure 3b allowing to evaluate the relative per-
 282 formance of the mechanistic model proposed by Eq. 20. COAREG is able to reproduce
 283 76% and 71% of the transfer velocities of CO₂ and DMS, respectively. The root mean
 284 square errors of the two models are overall of the same order of magnitude: 23.81 cm hr⁻¹
 285 for the breaking crest length based model and 24.41 cm hr⁻¹ for COAREG for CO₂ and
 286 DMS combined. Note that fixing \mathcal{A} using the DMS data assuming no bubble contribu-
 287 tion to its transfer ($k = \mathcal{A}K_\varepsilon$) and subsequently determining the other coefficients with
 288 the CO₂ data results in poorer fit statistics for DMS while not improving those for CO₂.

289 4 Discussion

290 4.1 Comparison to other mechanistic models

291 The base functional form of the model for k (Eq. 1) is a linear combination of pa-
 292 rameterizations of transfer velocities arising from different processes. As such, it follows
 293 the form adopted by previous studies (Deike and Melville, 2018; Fairall et al., 2011; Asher
 294 and Wanninkhof, 1998). Unlike in COAREG, it does not take into account the air-side
 295 transfer and is therefore only applicable to sparingly and less soluble gases. This could
 296 explain its poorer performance, particularly for DMS.

297 No distinction is made between the turbulence-mediated transfer due to wave break-
 298 ing and other processes as is done in Asher and Wanninkhof (1998); Shuiqing and Dongliang
 299 (2016). This is because computing the dissipation using the effective breaking strength
 300 gives an integrated estimate of the turbulence in the upper ocean at the given whitecap
 301 coverage and wave age. Indeed, b_{eff} was determined from the combination of breaking
 302 crest length distribution estimates and measures of the upper ocean turbulence that in-
 303 clude both the wave breaking turbulence and the background turbulence (Zappa et al.,
 304 2016).

305 The proportionality coefficient $\mathcal{A} = 0.211 \pm 0.034$ that multiplies K_ε to give k_ε is
 306 within the range of those determined in previous studies none of which account for bub-
 307 bles ($k = k_\varepsilon$). Zappa et al. (2007) suggested $\mathcal{A} = 0.4$ based on data collected in a large
 308 tidal river, a macro-tidal estuary, and from a coastal ocean site as well as in a “model”
 309 saltwater ocean at Biosphere 2 (Oracle, AZ USA). Later studies by Tokoro et al. (2008)
 310 suggest $\mathcal{A} = 0.17-0.18$ for riverine and coastal environments while Vachon et al. (2010)

311 determined $\mathcal{A} = 0.39-0.44$ in freshwater systems. The first open ocean verification of the
 312 functional form of k_ε suggest $\mathcal{A} = 0.12-1.46$ depending on the depth at which the tur-
 313 bulent kinetic dissipation rate measurements were taken and the approach used to ex-
 314 trapolate these measurements to the surface (Esters et al., 2017). Note that in this study
 315 different values of \mathcal{A} were determined for CO_2 and DMS as the transfer velocities of these
 316 gases cannot be reconciled without taking bubble-mediated transfer into account. While
 317 fitting the transfer velocities separately may have led to improved fit statistics, it would
 318 defeat the goal of finding an unified model for both if not all gases. Since \mathcal{A} depends on
 319 the measurement of ε at the surface and observations vary greatly over the depth that
 320 it is evaluated, direct comparison between studies is difficult. As shown in Zappa et al.
 321 (2009), the near-surface dissipation can vary several orders of magnitude in the top 50
 322 cm and will have a distinct impact on the gas transfer velocity. The value reported here
 323 is one corresponding to an integrated dissipation over the depth of the wave boundary
 324 layer roughly equal to the height of the wind-sea.

325 The form of the bubble-mediated transfer used in Asher and Wanninkhof (1998)
 326 could not be used for this study because 1) a wider variety of solubility have to be con-
 327 sidered to estimate the coefficients and there are more unknowns than gases available,
 328 and 2) it accounts for wave breaking only via W . Asher and Wanninkhof (1998) devel-
 329 oped their model using laboratory W which may have led to unrealistic estimates of both
 330 the bubble and the wave breaking turbulence mediate transfers. One could easily use the
 331 functional form proposed by Merlivat et al. (1993) for the bubble-mediated transfer with
 332 the coefficients determined by Asher and Wanninkhof (1998) to estimate K_b in Eq. 20.
 333 This however defeats the goal of a purely breaking crest length and sea state dependent
 334 model.

335 Both Woolf (1997), Woolf et al. (2007) and Goddijn-Murphy et al. (2016) assumed
 336 that the left and right hand side terms of Eq. 5 are equal rather than proportional. In
 337 both the model proposed herein and COAREG k_b scaling is adjusted through the em-
 338 pirical parameters \mathcal{B} and \mathcal{B}_{COAREG} , respectively. Note that these cannot be set inde-
 339 pendently from the models' the other adjustment constants. \mathcal{B}_{COAREG} further depends
 340 on the choice of the W parameterization. Its original value of 1.8 was tuned to the SO
 341 GasEx data using the Monahan and O'Muircheartaigh (1980) W parameterization which
 342 was shown to highly over estimate W at high wind speeds (Brumer et al., 2017b). Based
 343 on the HiWinGS data set, Blomquist et al. (2017) updated \mathcal{B}_{COAREG} to equal 3.8 which

344 is close to the value found in the present study. Although the same parameterization is
 345 at the base of the bubble-mediated transfer in the present framework and in COAREG,
 346 \mathcal{B} and \mathcal{B}_{COAREG} are not directly comparable as they depend on the measure of the bub-
 347 ble air volume flux (F_a) used and on χ (Eq. 7). The bubble air volume flux estimated
 348 here from the breaking crest length distribution is about twice as large as that computed
 349 in COAREG using 2450 W .

350 Values of these empirical factors are not independent and reflect the uncertainties
 351 in the breaking crest length derived statistics. The choice of U_b and B will impact \mathcal{B} and
 352 \mathcal{C} which further account for the fact that we are dealing with estimates of the integrated
 353 flux of bubble plumes without resolving variations in the bubble size distributions and
 354 the flux and lifetime of individual bubbles. The empirical constants \mathcal{A} and \mathcal{B} could be
 355 interpreted as efficiencies of the turbulent driven and bubble mediated transfer, respec-
 356 tively. \mathcal{C} encompasses the fact that full equilibration depends on the the limited volume
 357 of water between bubbles which is linked to the void fraction. A constant \mathcal{C} does not al-
 358 low for any variation (sea-state dependent or other) of the void fraction. A form of K_b
 359 including a breaking crest length dependent void fraction is derived in SI. It contains more
 360 unknowns and results in more scatter.

361 4.2 Remaining unknowns and limitations

362 Although the assumed functional form follows the typical approach used in other
 363 process based models, it may not be entirely correct. Indeed, it is not the gas transfer
 364 velocities that should be combined linearly, but rather the bubble- and turbulence-mediated
 365 fluxes ($F_g = F_\varepsilon + F_b$). The partial pressure of a gas within a bubble is higher than that
 366 in the atmosphere due to the pressure caused by the surface tension of the bubble skin,
 367 which can be estimated from the Young-Laplace equation and hydrostatic pressure of
 368 the surrounding water. Estimation of this excess pressure a bubble requires knowledge
 369 of the bubble size distribution as a function of depth and time.

370 The formulations of the bubble air volume flux contain several unknowns other than
 371 the bubble plume depth discussed above. The first unknown is the bubble cloud constant
 372 B which was set to 0.1 in accordance to Deike et al. (2016, 2017). B was determined from
 373 laboratory data from Duncan (1981), Lamarre and Melville (1991) and Deane and Stokes
 374 (2002) for time averaged volumes of air entrained \bar{V} by a single breaking wave ranging

375 several orders of magnitude ($10^{-7} < \bar{V} < 10^{-1} \text{ m}^3$). The relationship however does
 376 not hold for $\bar{V} < 10^{-5} \text{ m}^3$ and it is unclear how these scale for open ocean conditions.
 377 The other unknown is the dissipation-weighted vertical mean bubble plume rise veloc-
 378 ity (U_b). A constant U_b of 10 cm s^{-1} was used, corresponding to the rise terminal rise
 379 velocity of clean bubble of radius of $450 \mu\text{m}$ according to Woolf and Thorpe (1991). It
 380 is of the same order of magnitude as the rise velocity measured by Asher et al. (1997)
 381 in a sea-water tank which averaged around 8 cm s^{-1} within the first 6 seconds. Deike
 382 et al. (2017) proposed the following parameterization for U_b :

$$U_b \sim h/\tau_{br} \quad (22)$$

383 where h is the height of the wave at the time of breaking. While h is not measured di-
 384 rectly it may be approximated as the significant height of the wind-sea (H_{sws}). The pro-
 385 portionality factor has however yet to be established. Since H_{sws} ranges from ~ 0.1 to
 386 8 m and τ_{br} is on the order of $1\text{-}10 \text{ s}$, a proportionality coefficient equal to 1, as suggested
 387 by Deike et al. (2017), would lead to rise velocities ranging from a couple of centimeters
 388 a second to over a meter a second which is clearly too high.

389 Choosing a scale dependent U_b such as given by Eq. (22) would make F_a a func-
 390 tion of the 5th moment of $\Lambda(c)$ (c.f. Eq. 17). To date there is not enough independent
 391 evidence or a sound physical argument to rule on the validity of one formulation over
 392 the other. This is also true with regards to the approach taken here versus that of Deike
 393 and Melville (2018) whose F_a is a function of the 3rd moment of $\Lambda(c)$. The fundamen-
 394 tal difference is that they take a scale dependent $b(c)$ rather than b_{eff} based on the as-
 395 sumption that c_{br} may be related to a wavenumber through the deep water dispersion
 396 relation (Romero et al., 2012). Validity of this transformation has however been chal-
 397 lenged (Zappa et al., 2016; Banner et al., 2014).

398 Finally, throughout this framework, a Schmidt number exponent of $\frac{1}{2}$ is used (Eqs.
 399 (4), (5)) which is in accordance with open ocean scaling. The exponent was suggested
 400 to vary between $\frac{1}{2}$ for wavy, surfactant free conditions to $\frac{2}{3}$ for flat, film covered surfaces.
 401 The exponent may therefor need adjustment for coastal applications and other surfactant-
 402 influenced surface conditions. The impact of surface-active material on the framework's
 403 coefficients (\mathcal{A} , \mathcal{B} , \mathcal{C}) remains unknown.

5 Conclusions

A novel framework to model the gas transfer velocity of sparingly soluble gases under breaking wave conditions in the open ocean is presented herein. It allows for estimations based on the breaking crest length distributions and sea state. As such it is applicable to purely remotely sensed data. Tuned to measurements from the HiWinGS field campaign it performs comparably to the COAREG algorithms. Higher noise in breaking length derived statistics compared to whitecap and friction velocity estimates accounts for relatively poorer results of the breaking crest length dependent model compared to COAREG. Unknowns remain in the formulation of the bubble-mediated transfer as is the case with other physically based models put forward in the literature. Measurements of bubble plumes in the ocean are necessary for further improvement.

Acknowledgments

The authors acknowledge Dr. Gemmrich who provided the original Matlab code to breaking crest length tracking that was adapted to the HiWinGS data. The analysis for the HiWinGS project was funded by the National Science Foundation (Grants OCE-1537890). Data used in the analysis described here have been made available through NOAA's Physical Sciences Laboratory repository (<https://psl.noaa.gov/psd3/cruises/>). S. E. Brumer was supported by a postdoctoral grant of the Centre National d'Études Spatiales (CNES).

References

- Agrawal, Y. C., Terray, E. A., Donelan, M. A., Hwang, P. A., Williams III, A., Drennan, W. M., Kahma, K. K., and Kitaigorodskii, S. A. (1992). Enhanced dissipation of kinetic energy beneath surface waves. *Nature*, 359:219–20.
- Asher, W. E., Karle, L. M., and Higgins, B. J. (1997). On the differences between bubble-mediated air-water gas transfer in freshwater and seawater. *Journal of Marine Research*, 55:813–845.
- Asher, W. E., Karle, L. M., Higgins, B. J., Farley, P. J., Monahan, E. C., and Leifer, I. S. (1996). The influence of bubble plumes on air-seawater gas transfer velocities. *Journal Of Geophysical Research*, 101(C5):12027–12041.
- Asher, W. E. and Wanninkhof, R. (1998). The effect of bubble-mediated gas transfer on purposeful dual-gaseous tracer experiments. *Journal of Geophysical Research*, 103(C5):10555–60.

- 435 Atmane, M. A., Asher, W. E., and Jessup, A. T. (2004). On the use of the active
436 infrared technique to infer heat and gas transfer velocities at the air-water free
437 surface. *Journal of Geophysical Research*, 109:C08S14.
- 438 Banerjee, S., Lakehal, D., and Fulgosi, M. (2004). Surface divergence models for
439 scalar exchange between turbulent streams. *International Journal of Multiphase*
440 *Flow*, 30(7):963–977. A Collection of Papers in Honor of Professor G. Yadigaroglu
441 on the Occasion of his 65th Birthday.
- 442 Banerjee, S. and MacIntyre, S. (2004). The air-water interface: Turbulence and
443 scalar exchange. *Advances in coastal and ocean engineering*, 9:181.
- 444 Banerjee, S., Scott, D. S., and Rhodes, E. (1968). Mass transfer to falling wavy liq-
445 uid films in turbulent flow. *Industrial and Engineering Chemistry Fundamentals*,
446 7(1):22–27.
- 447 Banner, M. L. and Peirson, W. L. (2007). Wave breaking onset and strength for two-
448 dimensional deep-water wave groups. *Journal of Fluid Mechanics*, 585:93–115.
- 449 Banner, M. L., Zappa, C. J., and Gemmrich, J. (2014). A note on phillips’ spectral
450 framework for ocean whitecaps. *Journal of Physical Oceanography*, 44(7):1727–
451 1734.
- 452 Batchelor, G. K. (1959). Small-scale variation of convected quantities like tempera-
453 ture in turbulent fluid. part 1. general discussion and the case of small conductiv-
454 ity. *Journal of Fluid Mechanics*, 5:113–133.
- 455 Blomquist, B. W., Brumer, S. E., Fairall, C. W., Huebert, B. J., Zappa, C. J.,
456 Brooks, I. M., Yang, M., Bariteau, L., Prytherch, J., Hare, J. E., Czernski, H.,
457 Matei, A., and Pascal, R. W. (2017). Wind speed and sea state dependencies of
458 air-sea gas transfer: Results from the high wind speed gas exchange study (Hi-
459 WinGS). *Journal of Geophysical Research: Oceans*, 122(10):8034–8062.
- 460 Brumer, S. E., Zappa, C. J., Blomquist, B. W., Fairall, C. W., Cifuentes-Lorenzen,
461 A., Edson, J. B., Brooks, I. M., and Huebert, B. J. (2017a). Wave-related reynolds
462 number parameterizations of CO₂ and DMS transfer velocities. *Geophysical Re-*
463 *search Letters*, 44(19):9865–9875. 2017GL074979.
- 464 Brumer, S. E., Zappa, C. J., Brooks, I. M., Tamura, H., Brown, S. M., Blomquist,
465 B., Fairall, C. W., and Cifuentes-Lorenzen, A. (2017b). Whitecap coverage de-
466 pendence on wind and wave statistics as observed during so gasex and hiwings.
467 *Journal of Physical Oceanography*.

- 468 Cipriano, R. and Blanchard, D. (1981). Bubble and aerosol spectra produced by a
469 laboratory "breaking wave". *Journal of Geophysical Research*, 86:8085–8092.
- 470 Danckwerts, P. V. (1951). Significance of liquid-film coefficients in gas absorption.
471 *Industrial and Engineering Chemistry*, 43(6):1460–1467.
- 472 Deane, G. B. and Stokes, M. D. (2002). Scale dependence of bubble creation mecha-
473 nisms in breaking waves. *Nature*, 418(6900):839–844.
- 474 Deike, L. (2022). Mass transfer at the ocean-atmosphere interface: The role of wave
475 breaking, droplets, and bubbles. *Annual Review of Fluid Mechanics*, 54(1):null.
- 476 Deike, L., Lenain, L., and Melville, W. K. (2017). Air entrainment by breaking
477 waves. *Geophysical Research Letters*, 44(8):3779–3787. 2017GL072883.
- 478 Deike, L. and Melville, W. K. (2018). Gas transfer by breaking waves. *Geophysical
479 Research Letters*, 45(19):10,482–10,492.
- 480 Deike, L., Melville, W. K., and Popinet, S. (2016). Air entrainment and bubble
481 statistics in breaking waves. *Journal of Fluid Mechanics*, 801:91–129.
- 482 Drazen, D. A., Melville, W. K., and Lenain, L. (2008). Inertial scaling of dissipation
483 in unsteady breaking waves. *Journal of Fluid Mechanics*, 611:307–332.
- 484 Duncan, J. H. (1981). An experimental investigation of breaking waves produced
485 by a towed hydrofoil. *Proceedings of the Royal Society of London, Series A*,
486 377(1770):331–48.
- 487 Duncan, J. H. (1983). The breaking and non-breaking wave resistance of a two-
488 dimensional hydrofoil. *Journal of Fluid Mechanics*, 126:507–20.
- 489 Esters, L., Landwehr, S., Sutherland, G., Bell, T. G., Christensen, K. H., Saltzman,
490 E. S., Miller, S. D., and Ward, B. (2017). Parameterizing air-sea gas transfer
491 velocity with dissipation. *Journal of Geophysical Research: Oceans*, 122(4):3041–
492 3056.
- 493 Fairall, C. W., Yang, M., Bariteau, L., Edson, J. B., Helmig, D., McGillis, W., Pe-
494 zoa, S., Hare, J. E., Huebert, B., and Blomquist, B. (2011). Implementation of the
495 coupled ocean-atmosphere response experiment flux algorithm with CO₂, dimethyl
496 sulfide, and O₃. *Journal of Geophysical Research*, 116(C00F09):C00F09.
- 497 Gemmrich, J. R. (2010). Strong turbulence in the wave crest region. *J. Phys.
498 Oceanogr.*, 40:583–595.
- 499 Gemmrich, J. R., Banner, M. L., and Garrett, C. (2008). Spectrally resolved energy
500 dissipation and momentum flux of breaking waves. *J. Phys. Oceanogr.*, 38:1296–

- 501 1312.
- 502 Gemmrich, J. R., Zappa, C. J., Banner, M. L., and Morison, R. P. (2013). Wave
503 breaking in developing and mature seas. *Journal of Geophysical Research -*
504 *Oceans*, 118:4542–4552.
- 505 Goddijn-Murphy, L., Woolf, D. K., Callaghan, A. H., Nightingale, P. D., and Shut-
506 ler, J. D. (2016). A reconciliation of empirical and mechanistic models of the
507 air-sea gas transfer velocity. *Journal of Geophysical Research: Oceans*, 121(1):818–
508 835.
- 509 Harriott, P. (1962). A random eddy modification of the penetration theory. *Chemical*
510 *Engineering Science*, 17:149–154.
- 511 Higbie, R. (1935). The rate of absorption of a pure gas into a still liquid during
512 short periods of exposure. *Trans. A.I.C.E.*, 31:365–389.
- 513 Ho, D., Sabine, C. L., Hebert, D., Ullman, D. S., Wanninkhof, R., Hamme, R. C.,
514 Strutton, P. G., Hales, B., Edson, J. B., and Hargreaves, B. R. (2011). South-
515 ern ocean gas exchange experiment: Setting the stage. *Journal of Geophysical*
516 *Research - Oceans*, 116(C4):C00F08.
- 517 Keeling, R. F. (1993). On the role of large bubbles in air-sea gas exchange and su-
518 persaturation in the ocean. *J. Mar. Res.*, 51:237–271.
- 519 Kitaigorodskii, S. A. (1984). On the fluid dynamical theory of turbulent gas trans-
520 fer across an air-sea interface in the presence of breaking wind-waves. *Journal of*
521 *Physical Oceanography*, 14(5):960–972.
- 522 Kleiss, J. M. (2009). *Airborne observations of the kinematics and statistics of break-*
523 *ing waves*. PhD thesis, Scripps Institution of Oceanography-University of Califor-
524 nia.
- 525 Kleiss, J. M. and Melville, W. K. (2010). Observations of wave breaking kinematics
526 in fetchlimited seas. *J. Phys. Oceanogr.*, 40:2575–2604.
- 527 Komori, S., Nagaosa, R., and Murakami, Y. (1993). Turbulence structure and heat
528 and mass transfer mechanism at a gas-liquid interface in a wind-wave tunnel. *Ap-*
529 *plied Scientific Research*, 51:423–427.
- 530 Lamarre, E. and Melville, W. K. (1991). Air entrainment and dissipation in breaking
531 waves. *Nature*, 351(6326):469–72.
- 532 Lamont, J. C. and Scott, D. S. (1970). An eddy cell model of mass transfer into the
533 surface of a turbulent liquid. *A.I.Ch.E. J.*, 16:512–519.

- 534 Liang, J.-H., Deutsch, C., McWilliams, J. C., Baschek, B., Sullivan, P. P., and
535 Chiba, D. (2013). Parameterizing bubble-mediated air-sea gas exchange and
536 its effect on ocean ventilation. *Global Biogeochemical Cycles*, 27(3):894–905.
- 537 McCreedy, M. J., Vassiliadou, E., and Hanratty, T. J. (1986). Computer simulation
538 of turbulent mass transfer at a mobile interface. *AIChE Journal*, 32(7):1108–1115.
- 539 McKenna, S. P. and McGillis, W. R. (2004). Observations of flow repeatability
540 and secondary circulation in an oscillating grid-stirred tank. *Physics of Fluids*,
541 16(9):3499–3502.
- 542 Melville, W. K. (1994). Energy dissipation by breaking waves. *Journal of Physical*
543 *Oceanography*, 24(10):2041–9.
- 544 Merlivat, L., Memery, L., and Boutin, J. (1993). Gas exchange at the air-sea in-
545 terface: present status. case of CO₂. In *The Fourth International Conference on*
546 *CO₂ in the Oceans Inst. Natl. des Sci. de l’Univers., Cent. Natl. de la Rech. Sci.*
547 *Carqueiranne, France Sept*, pages 13–17.
- 548 Monahan, E. C. and O’Muircheartaigh, I. (1980). Optimal power-law description
549 of oceanic whitecap coverage dependence on wind speed. *Journal of Physical*
550 *Oceanography*, 10(12):2064–2099.
- 551 Phillips, O. M. (1985). Spectral and statistical properties of the equilibrium range in
552 wind-generated gravity waves. *Journal of Fluid Mechanics*, 156:505–31.
- 553 Phillips, O. M., Posner, F. L., and Hansen, J. P. (2001). High range resolution
554 radar measurements of the speed distribution of breaking events in wind-generated
555 ocean waves: Surface impulse and wave energy dissipation rates. *Journal of Physi-*
556 *cal Oceanography*, 31(2):450–460.
- 557 Rapp, R. J. and Melville, W. K. (1990). Laboratory measurements of deep-water
558 breaking waves. *Philosophical Transactions of the Royal Society of London A*,
559 331(1622):735–800.
- 560 Romero, L., Melville, W. K., and Kleiss, J. (2012). Spectral energy dissipation due
561 to surface-wave breaking. *J. Phys. Oceanogr.*, pages 1421–1444.
- 562 Schwendeman, M., Thomson, J., and Gemmrich, J. R. (2014). Wave breaking and
563 dissipation in a young wind sea. *Journal of Physical Oceanography*, 44(1):104–127.
- 564 Shuiqing, L. and Dongliang, Z. (2016). Gas transfer velocity in the presence of wave
565 breaking. *Tellus B: Chemical and Physical Meteorology*, 68(1):27034.

- 566 Sutherland, P. and Melville, W. K. (2013). Field measurements and scaling of ocean
567 surface wave-breaking statistics. *Geophysical Research Letters*, 40:3074–3079.
- 568 Sutherland, P. and Melville, W. K. (2015). Field measurements of surface and near-
569 surface turbulence in the presence of breaking waves. *Journal of Physical Oceanog-
570 raphy*, 45(4):943–965.
- 571 Terray, E. A., Donelan, M. A., Agrawal, Y. C., Drennan, W. M., Kahma, K. K.,
572 A. J. Williams, I., Hwang, P. A., and Kitaigorodskii, S. A. (1996). Estimates of
573 kinetic energy dissipation under surface waves. *Journal of Physical Oceanography*,
574 26(5):792–807.
- 575 Thomson, J., Gemmrich, J. R., and Jessup, A. T. (2009). Energy dissipation and the
576 spectral distribution of whitecaps. *Geophys. Res Lett.*, 35:L11601.
- 577 Thorpe, S. A. and Hall, A. J. (1983). The characteristics of breaking waves, bubble
578 clouds, and near-surface currents observed using side-scan sonar. *Continental Shelf
579 Research*, 1(4):353–384.
- 580 Tokoro, T., Kayanne, H., Watanabe, A., Nadaoka, K., Tamura, H., Nozaki, K.,
581 Kato, K., and Negishi, A. (2008). High gas-transfer velocity in coastal regions
582 with high energy-dissipation rates. *Journal of Geophysical Research: Oceans*,
583 113(C11):C11006.
- 584 Turney, D. E., Smith, W. C., and Banerjee, S. (2005). A measure of the near-surface
585 fluid motions that predicts air-water gas transfer in a wide range of conditions.
586 *Geophysical Research Letters*, 32:L04607.
- 587 Vachon, D., Prairie, Y. T., and Cole, J. J. (2010). The relationship between near-
588 surface turbulence and gas transfer velocity in freshwater systems and its im-
589 plications for floating chamber measurements of gas exchange. *Limnology and
590 Oceanography*, 55(4):1723–1732.
- 591 Wanninkhof, R. (1992). Relationship between wind speed and gas exchange over the
592 ocean. *Journal of Geophysical Research*, 97(C5):7373–7382.
- 593 Woolf, D. K. (1993). Bubbles and the air-sea transfer velocity of gases. *Atmos.
594 Ocean*, 31:517–540.
- 595 Woolf, D. K. (1997). *Bubbles and their role in air-sea gas exchange*, pages 173–206.
596 Cambridge Univ Press, Cambridge, UK.
- 597 Woolf, D. K., Leifer, I. S., Nightingale, P. D., Rhee, T. S., Bowyer, P., Caulliez,
598 G., de Leeuw, G., Larsen, S. E., Liddicoat, M., Baker, J., and Andreae, M. O.

- 599 (2007). Modelling of bubble-mediated gas transfer: Fundamental principles and a
600 laboratory test. *Journal of Marine Systems*, 66(1-4):71–91.
- 601 Woolf, D. K. and Thorpe, S. A. (1991). Bubbles and the air-sea exchange of gases in
602 near saturation conditions. *J. Mar. Res.*, 49:435–466.
- 603 Yang, M., Blomquist, B., and Nightingale, P. D. (2014). Air-sea exchange of
604 methanol and acetone during hiwings: Estimation of air phase, water phase gas
605 transfer velocities. *Journal of Geophysical Research: Oceans*, 119(10):7308–7323.
- 606 Zappa, C. J., Banner, M. L., Gemmrich, J. R., Schultz, H., Morison, R. P., LeBel,
607 D. A., and Dickey, T. (2012). An overview of sea state conditions and air-sea
608 fluxes during radyo. *Journal of Geophysical Research - Oceans*, 117:C00H19.
- 609 Zappa, C. J., Banner, M. L., Morison, R. P., and Brumer, S. E. (2016). On the vari-
610 ation of the effective breaking strength in oceanic sea states. *Journal of Physical
611 Oceanography*, 46(7):2049–2061.
- 612 Zappa, C. J., Ho, D. T., McGillis, W. R., Banner, M. L., Dacey, J. W. H., Bliven,
613 L. F., Ma, B., and Nystuen, J. (2009). Rain-induced turbulence and air-sea gas
614 transfer. *Journal Of Geophysical Research Oceans*, 114:C07009.
- 615 Zappa, C. J., McGillis, W. R., Raymond, P. A., Edson, J. B., Hints, E. J., Zem-
616 melink, H. J., Dacey, J. W. H., and Ho, D. T. (2007). Environmental turbulent
617 mixing controls on the air-water gas exchange in marine and aquatic systems.
618 *Geophysical Research Letters*, 34(L10601):doi:10.1029/ 2006GL028790.

Supporting Information for ”A novel wave breaking framework to estimate air-sea gas transfer velocities”

Sophia E. Brumer^{1,a}, Christopher J. Zappa¹

¹Lamont-Doherty Earth Observatory of Columbia University, Palisades, NY, USA.

^aNow at Laboratoire d’Océanographie Physique et Spatiale, UMR 6523 CNRS-IFREMER-IRD-UBO, IUEM, Plouzané, France

Contents of this file

1. Text S1 to S4
2. Figures S1 to S2

Introduction

Text S1 provides more details regarding the breaking crest detection and tracking algorithm which should be sufficient to replicate it. It lists the functions of the Matlab image processing toolbox used. Note that the algorithm should be adapted to the spatial resolution of the imagery it is applied on.

Text S2 provides the equation for breaking crest length distribution scalings proposed in the literature (Deike and Melville, 2018; Sutherland and Melville, 2013). Both are based on the same dataset. Deike and Melville (2018) proposed a simplified form which is plotted in Figure S1 for HiWinGS conditions along with the breaking crest length distribution

determined in this study. A poor correspondence between the HiWinGS data and the scaling can be observed which may stem from the fundamentally different way breaking crest length distribution were computed in this study and those from which the scalings were derived. Addressing the difference is an active area of research which goes beyond the scope of this publication.

Text S3 recalls the main equations of the NOAA-COAREG algorithm. These can be found in Blomquist et al. (2017); Fairall et al. (2011) and references therein.

Text S4 discusses an alternate formulation of the bubble mediate transfer which accounts for suffocation which may occur in dense bubble plumes. It depends on an additional bubble plume characteristic which may be estimated from breaking crest length distribution and sea state statistics: the void fraction. Related geometric consideration of breaking waves and associated bubble plumes are illustrated in Figure S2. Due to an increased number of unknowns and scatter in results this formulation was not retained for the main framework.

Text S1. Steps of the breaking crest detection and tracking algorithm

1. Intrinsic and extrinsic image correction is applied to the images of a given video (frequency down-sampling is applied in this loop) which are re-gridded onto a regular x,y grid resulting in an image matrix $I(t, x, y)$ where t is the time dimension time
2. This matrix is differences with respect of time: $diffI = I(2:end, :, :) - I(1:end-1, :, :)$
3. diffI is converted into a binary matrix (1 for advancing crest, 0 for rest) based on an intensity threshold: $BW = im2bw(diffI./max(diffI(:)), 0.6)$
4. Holes are filled using $BW = imfill(BW, 'holes')$
5. The features in the image are dilated using $BW = imdilate(BW, strel('diamond', 10))$
6. Pixels separated by only 1 pixel are connected using : $BW = bwmorph(BW, 'bridge')$
7. Pixels are set to 1 if at least 5 pixels within a 3x3 neighbouring area are 1, if not they are set to 0 using: $BW = bwmorph(BW, 'bridge')$
8. Holes are filled $BW = imfill(BW, 'holes')$
9. The features in the image are eroded using $imerode(BW, strel('diamond', 5))$
10. Individual features are identified and labeled: $[L, NO] = bwlabeln(BW, 8);$
11. Region properties (area, orientation) are computed $L_props = regionprops(L, 'area', 'orientation')$
12. Only features greater than the chosen area threshold (AreaThresh) are kept and labels are re-assigned: $BW = ismember(L, find([L_props.Area] > AreaThresh)); [L, NO] = bwlabeln(BW, 8)$
13. Breaking crests are tracked from one differenced image pair to the next by matching features that evolve corresponding to the criterion mentioned in section 3.1.

Text S2. Lambda scaling

Two scalings have been proposed for $\Lambda(c)$ for $c > c_{min}$ assuming a c^{-6} tail:

1. Deike and Melville (2018):

$$\Lambda(c) = 0.25 \frac{g}{\sqrt{gH_s}^3} \left(\frac{c}{\sqrt{gH_s}} \right)^{-6} \left(\frac{u_*}{\sqrt{gH_s}} \right)^{5/3} \quad (\text{S1})$$

$$c_{min} = 0.85 \sqrt{gH_s} \quad (\text{S2})$$

2. Sutherland and Melville (2013):

$$\Lambda(c) = \frac{g}{c_p^3} \sqrt{\frac{u_*}{c_p}} \frac{c}{gH_s} \left(\frac{gH_s}{c_p^2} \right)^{0.1} \quad (\text{S3})$$

Figure S1 show how the scaling of Deike and Melville (2018) for the HiWinGS sea state conditions compares to the imagery derived breaking crest length distribution.

Text S3. The NOAA-COAREG algorithm

The key equations of the NOAA-COAREG algorithm are recalled in the following section. These were published in Blomquist et al. (2017); Fairall et al. (2011) and references therein. The gas transfer velocity is composed of an air- ($1/k_a$) and a water-side resistance ($1/k_w$):

$$k = (\alpha/k_a + 1/k_w)^{-1} \quad (\text{S4})$$

The air-side transfer depends on the air friction velocity (u_*), the atmospheric velocity drag coefficient (C_d), and the Schmidt number for the gas in the air (Sc_a).

$$k_a = u_*/ \left(13.3Sc_a^{1/2} + C_d^{1/2} - 5 + \ln(Sc_a)/(2\kappa) \right) \quad (\text{S5})$$

The water-side transfer is composed of a turbulent molecular transfer (k_{wt}) and a bubble mediated (k_b) one:

$$k_w = k_{wt} + k_b \quad (\text{S6})$$

The turbulent molecular transfer formulation takes the cool skin buoyancy driven transfer at low wind though an empirical function Φ in addition to effects of the tangential wind stress:

$$k_{wt} = u_*/(\rho_w/\rho_a)^{1/2} / \left(13.3/(\mathcal{A}_{COAREG}\Phi)Sc^{1/2} + \ln(z_w/\delta_w)/\kappa \right) \quad (\text{S7})$$

Here z_w is set to 0.5 and the Schmidt number of the gas in water (Sc) to 660. The cool-skin thickness, δ_w , is computed in the iterative loop of the COARE algorithm as is Φ .

The bubble mediated transfer formulation is that of Woolf (1997):

$$k_b = \mathcal{B}_{COAREG} \times 2450W\alpha^{-1} \left(1 + (14\alpha Sc^{-0.5})^{1/1.2} \right)^{-1.2} \quad (\text{S8})$$

The whitecap fraction W is parameterized as a function of wave-wind Reynolds number following Brumer et al. (2017):

$$W = 4.48 \times 10^{-6} \left(\frac{u_* H_s}{\nu_w} \right)^{0.90} / 100 \quad (\text{S9})$$

The two adjustment factors \mathcal{A}_{COAREG} and \mathcal{B}_{COAREG} are set to 1.2 and 3.8, respectively, based on the HiWinGS measurements (Blomquist et al., 2017).

Text S4. Accounting for suffocation

The model based on Eq. 5 does not account for the potential “suffocation” effect of bubbles within dense clouds. This effect was suggested to arise from the fact that bubbles evolve within a finite volume of water with relatively small interstitial space which has limited capacity to take up gases, thus restricting the bubble-mediated transfer (Woolf et al., 2007). An alternate form for k_b , labeled as the “dense plume model” was therefore proposed:

$$k_{b_{void}} \propto W \times X \frac{F_{a_{1\%}}}{\alpha} (1 + (X\chi)^{1/1.2})^{-1.2} \quad (\text{S10})$$

with

$$X = \alpha F_{w_{1\%}} / (\alpha F_{w_{1\%}} + F_{a_{1\%}}) \quad (\text{S11})$$

$F_{a_{1\%}}$ is the volume flux of air for 1% whitecap cover, i.e $F_{a_{1\%}} = F_a/W$, which Woolf et al. (2007) set to equal 24.5 cm hr⁻¹. $F_{w_{1\%}}$ is the volume flux of water within bubble plume relative to $F_{a_{1\%}}$ and is related to $F_{a_{1\%}}$ through the void fraction:

$$v = \frac{F_{a_{1\%}}}{F_{a_{1\%}} + F_{w_{1\%}}}. \quad (\text{S12})$$

Thus:

$$F_{w_{1\%}} = \frac{F_{a_{1\%}}}{v} - F_{a_{1\%}} \quad (\text{S13})$$

and

$$X = \frac{\alpha/v + \alpha}{\alpha/v + \alpha + 1} \quad (\text{S14})$$

The void fraction for a given breaking wave (v_{br}) can be estimated from V_a , the surface area of active breaking (A_{br}), which is proportional to the breaking crest length times

the “swept out” length of the breaker ($L_{br} \times c_{br} t_{br}$, see Figure S2), and the depth of the bubble plume (h):

$$v_{br} = \frac{V_a}{A_{br} h} = b_{eff} \frac{B}{U_b g^2} \frac{L_{br} c_{br}^5}{L_{br} c_{br} t_{br} h} = b_{eff} \frac{B}{U_b g^2} \frac{c_{br}^4}{t_{br} h} \quad (\text{S15})$$

The time averaged void fraction is then:

$$\bar{v} = \frac{\sum v_{br} t_{br}}{T} \quad (\text{S16})$$

The bubble plume depth remains elusive, but may be assumed to be proportional to the significant wave height of the wind-sea ($H_{s_{ws}}$) or to the “swept out” length of the breaker ($c_{br} t_{br}$). Figure S2 illustrates the assumed geometry of a plunging breaker and the subsequent bubble plume. Recent work (Cifuentes-Lorenzen et al., 2020) suggests that the peak wave number k_p is a better predictor for the bubble plume depths based on acoustic backscatter measurements due to breaking waves in the Southern Ocean.

The three estimates are then given by:

1. assuming $h \propto H_{s_{ws}}$ (e.g., Rapp and Melville, 1990; Lamarre and Melville, 1991; Baldy and Bourguel, 1987):

$$\bar{v} \propto \frac{b_{eff} B}{H_{s_{ws}} T U_b g^2} \sum c_{br}^4. \quad (\text{S17})$$

2. assuming $h \propto c_{br} t_{br}$ (e.g., Deike et al., 2016):

$$\bar{v} \propto \frac{b_{eff} B}{T U_b g^2} \sum \frac{c_{br}^3}{t_{br}}. \quad (\text{S18})$$

3. assuming $h \propto f(k_p)$:

$$\bar{v} \propto \frac{b_{eff} B}{f(k_p) T U_b g^2} \sum c_{br}^4. \quad (\text{S19})$$

Note that all three forms are independent of the breaking crest length and cannot be expressed in terms of moments of the breaking crest length distribution. They are however

straight forward to determine from the imagery during the processing to obtain $\Lambda(c)$. In light of recent modeling advances (Romero, 2019), breaking crest length distribution dependant formulations are of higher interest to the community. What is more, Eq. S10 contains more uncertainties than Eq. 5). Using the right hand side of Eq. S10, with the void fraction estimated based any of the above equations instead of K_b leads to very poor overall correlations ($r^2 \sim 0.1$) on account of the large scatter in \bar{v} .

References

- Baldy, S. and Bourguel, M. (1987). Bubbles between the wave trough and wave crest levels. *Journal of Geophysical Research: Oceans*, 92(C3):2919–2929.
- Blomquist, B. W., Brumer, S. E., Fairall, C. W., Huebert, B. J., Zappa, C. J., Brooks, I. M., Yang, M., Bariteau, L., Prytherch, J., Hare, J. E., Czerski, H., Matei, A., and Pascal, R. W. (2017). Wind speed and sea state dependencies of air-sea gas transfer: Results from the high wind speed gas exchange study (HiWinGS). *Journal of Geophysical Research: Oceans*, 122(10):8034–8062.
- Brumer, S. E., Zappa, C. J., Brooks, I. M., Tamura, H., Brown, S. M., Blomquist, B., Fairall, C. W., and Cifuentes-Lorenzen, A. (2017). Whitecap coverage dependence on wind and wave statistics as observed during so gasex and hiwings. *Journal of Physical Oceanography*.
- Cifuentes-Lorenzen, A., Zappa, C. J., Randolph, K. L., and Edson, J. B. (2020). Scaling the bubble penetration depth in the open ocean during the southern ocean gas exchange experiment 2008. In *Ocean Sciences Meeting*.
- Deike, L. and Melville, W. K. (2018). Gas transfer by breaking waves. *Geophysical Research Letters*, 45(19):10,482–10,492.
- Deike, L., Melville, W. K., and Popinet, S. (2016). Air entrainment and bubble statistics in breaking waves. *Journal of Fluid Mechanics*, 801:91–129.
- Fairall, C. W., Yang, M., Bariteau, L., Edson, J. B., Helmig, D., McGillis, W., Pezoa, S., Hare, J. E., Huebert, B., and Blomquist, B. (2011). Implementation of the coupled ocean-atmosphere response experiment flux algorithm with CO₂, dimethyl sulfide, and

O₃. *Journal of Geophysical Research*, 116(C00F09):C00F09.

Lamarre, E. and Melville, W. K. (1991). Air entrainment and dissipation in breaking waves. *Nature*, 351(6326):469–72.

Rapp, R. J. and Melville, W. K. (1990). Laboratory measurements of deep-water breaking waves. *Philosophical Transactions of the Royal Society of London A*, 331(1622):735–800.

Romero, L. (2019). Distribution of surface wave breaking fronts. *Geophysical Research Letters*, 46(17-18):10463–10474.

Sutherland, P. and Melville, W. K. (2013). Field measurements and scaling of ocean surface wave-breaking statistics. *Geophysical Research Letters*, 40:3074–3079.

Woolf, D. K. (1997). *Bubbles and their role in air-sea gas exchange*, pages 173–206. Cambridge Univ Press, Cambridge, UK.

Woolf, D. K., Leifer, I. S., Nightingale, P. D., Rhee, T. S., Bowyer, P., Caulliez, G., de Leeuw, G., Larsen, S. E., Liddicoat, M., Baker, J., and Andreae, M. O. (2007). Modelling of bubble-mediated gas transfer: Fundamental principles and a laboratory test. *Journal of Marine Systems*, 66(1-4):71–91.

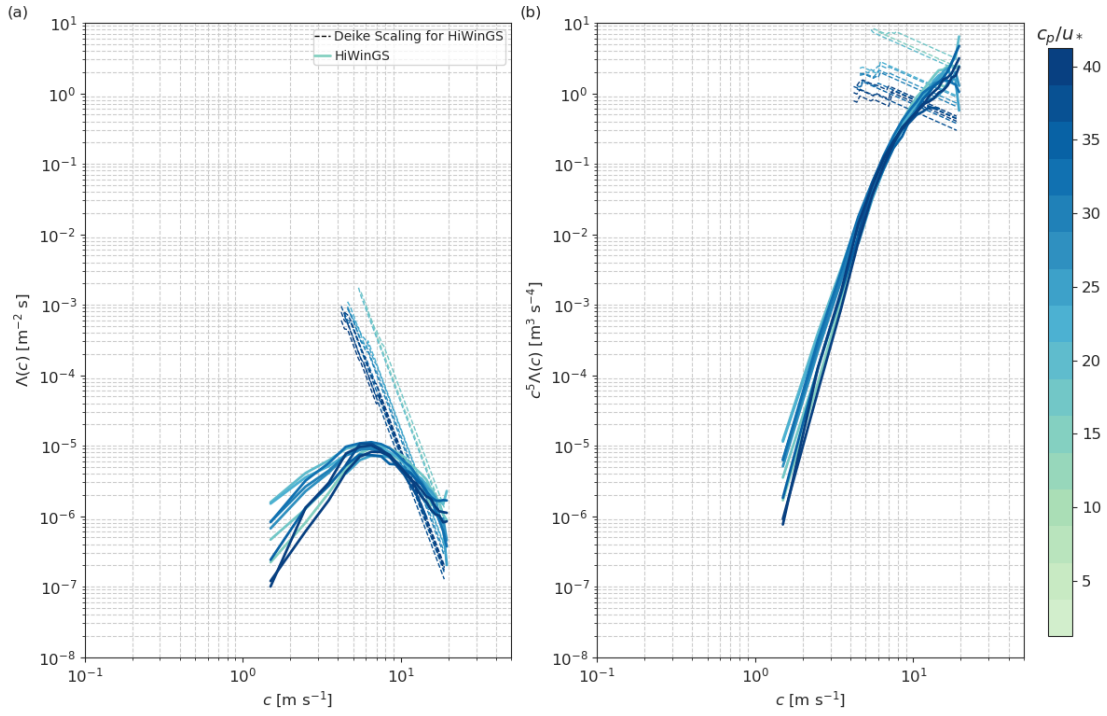
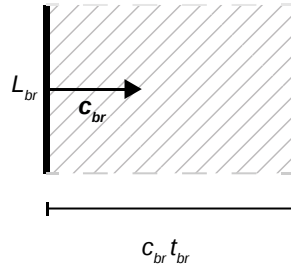


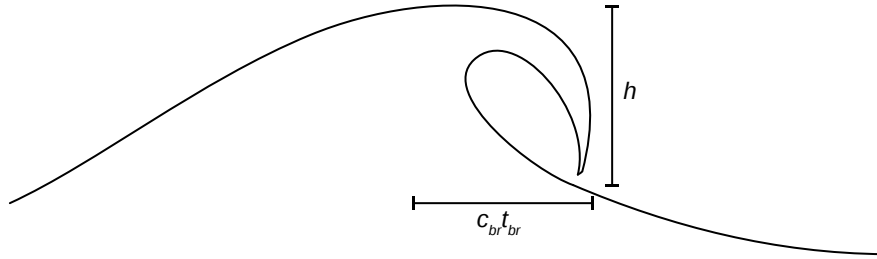
Figure S1. (a) Breaking crest length distributions and (b) their fifth moment as a function of the breaking crest speed color-coded by wave age ($\frac{c_p}{u_*}$). The HiWinGS data is plotted in solid lines while the corresponding Deike and Melville (2018) scaling is in dashed lines.

(a) Top View



(b) Side view of a plunging breaker

(1) Pre breaking



(2) Post breaking

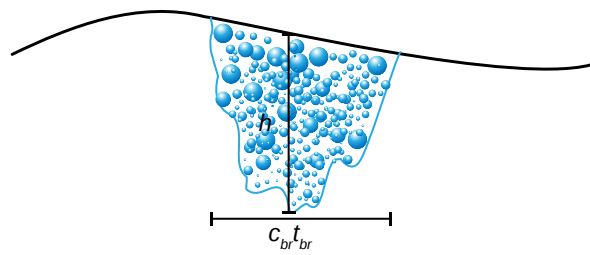


Figure S2. Sketch illustrating (a) the assumption that the swept out area is related to the length of breaking L_{br} , the translation $c_{br}t_{br}$ and (b) the assumed geometry of (1) a plunging breaker, and (2) the subsequent bubble plume.